Original Article

In silico screening of potential anti-inflammatory compounds from Sulawesi-endemic *Begonia medicinalis*

Ni KD. Permatasari[1*], Sri Wahyuningsih[2], Felisitas M. Podhi[1], Radinal Kautsar[1], Moh R. Afnani[1], Rizky D. Susetyo[2], Emilia J. Bria[2], Melania Priska[2], Florian MPR. Makin[2], Dece E. Sahertian[2], Anisa H. Uno[1] and Inez Maylida[1]

[1]Graduate Program in Biology, Department of Tropical Biology, Faculty of Biology, Universitas Gadjah Mada, Yogyakarta, Indonesia; [2]Doctoral Program in Biology, Department of Tropical Biology, Faculty of Biology, Universitas Gadjah Mada, Yogyakarta, Indonesia

*Corresponding author: nikadekdewipermatasari1999@mail.ugm.ac.id

Abstract

Chronic inflammation contributes to the pathogenesis of many degenerative diseases. Long-term use of conventional anti-inflammatory drugs may be associated with serious adverse effects, prompting the search for new natural candidates. *Begonia medicinalis* is a plant endemic to Central Sulawesi that is traditionally used to treat fever and joint pain, but its phytochemical profile and molecular mechanisms underlying its potential anti-inflammatory activity have not been scientifically reported. The aim of this study was to identify the secondary metabolite profile of the ethanol extract of *B. medicinalis* leaves and to assess its molecular interactions with pivotal pro-inflammatory targets, namely cyclooxygenase-2 (COX-2), inducible nitric oxide synthase (iNOS), tumor necrosis factor-alpha (TNF-α), and interleukin-1 beta (IL-1β), using a computational approach. The study combined a laboratory-based phytochemical analysis with in silico analyses, including structure-activity relationship (SAR), absorption, distribution, metabolism, and excretion (ADME), toxicity prediction, molecular docking, and molecular dynamics simulations. *B. medicinalis* leaves were extracted by maceration using absolute ethanol, and the metabolite profiles were analyzed using gas chromatography-mass spectrometry (GC-MS). Biological activity prediction was performed using PASS Online, pharmacokinetic profiling using SwissADME, toxicity evaluation using ProTox 3.0, and protein-protein interaction analysis using STRING v12.0. Molecular docking was performed using PyRx with AutoDock Vina and visualized using BIOVIA Discovery Studio 2025. GC-MS analysis identified 21 compounds, including palmitic acid, dihomo-γ-linolenic acid, and stigmasterol, which showed predicted anti-inflammatory potential, favorable safety profiles, and acceptable drug-likeness characteristics. Among these compounds, stigmasterol showed favorable predicted binding affinities toward COX-2, iNOS, TNF-α, and IL-1β, while molecular dynamics simulations supported the stability of the resulting complexes over 100 ns. These computational findings suggest that *B. medicinalis* contains diverse bioactive compounds with potential anti-inflammatory properties. Stigmasterol emerged as the most promising lead candidate against the predicted anti-inflammatory targets, providing a theoretical molecular foundation for the future exploration of *B. medicinalis* therapeutic potential.

Keywords: Anti-inflammatory, *Begonia medicinalis*, GC-MS, in silico, molecular docking

Introduction

Chronic inflammation is the pathophysiological driver of various degenerative and autoimmune diseases that pose a significant global health burden [1,2]. While conventional anti-inflammatory

Received: May 18, 2026 - Revised: August 19, 2026 - Accepted: August 21, 2026 - Published online: August 31, 2026

medications like nonsteroidal anti-inflammatory drugs (NSAIDs) and corticosteroids have been utilized for an extended period, their prolonged usage frequently induces significant adverse effects, ranging from nephrotoxicity to metabolic disorders [1,3,4]. These limitations underscore the urgent need to identify new and safer anti-inflammatory drug candidates with consistent efficacy for long-term therapy.

The Wallacea region, particularly Sulawesi, presents significant opportunities for the discovery of new bioactive compounds, owing to its remarkably high degree of floral endemism. A notable genus is *Begonia*, of which 62 of the 65 species in Sulawesi are endemic, with many considered endangered [5,6]. This local diversity offers considerable potential for bioprospecting; however, the phytochemical profiles and molecular mechanisms of many of these endemic plants remain largely undocumented in the scientific literature, highlighting their potential as an underexplored source of bioactive compounds for pharmaceutical research.

Begonia medicinalis Ardi & D.C. Thomas, known locally as "Benalu Batu", is a species endemic to Central Sulawesi that is traditionally used to treat fever, joint pain, and other inflammation-related disorders [7-10]. This species is known to be rich in secondary metabolites, including flavan-3-ol type flavonoids, polyphenols, and alkaloids, which may exhibit significant bioactive properties [8-11]. However, in-depth studies linking the specific metabolite profile of *B. medicinalis* to key inflammatory molecular targets remain very limited, and further mechanistic validation is warranted.

In modern drug discovery, precision medicine strategies highlight the need for selective interventions targeting key pro-inflammatory mediators, including cyclooxygenase-2 (COX-2), inducible nitric oxide synthase (iNOS), tumor necrosis factor-alpha (TNF-α), and interleukin-1 beta (IL-1β), while minimizing disruption of physiological immune functions [1,4,12,13]. The selection of TNF-α and IL-1β, which are cytokines rather than conventional enzymes with well-defined catalytic sites, was based on their central roles in inflammatory signaling and previous structural analyses suggesting the presence of surface cavities and receptor-binding interfaces that may accommodate small molecules. Molecular docking was therefore used to evaluate the potential binding of phytochemicals to reported ligand-binding regions or relevant protein interfaces rather than to infer direct cytokine inhibition [12,13]. Comprehensive in silico analyses, including structure-activity relationship (SAR), absorption, distribution, metabolism, and excretion (ADME), toxicity prediction, molecular docking, and molecular dynamics simulations, provide an efficient strategy for screening and prioritizing candidate compounds. These computational methods can help identify compounds with favorable predicted profiles for subsequent experimental evaluation in a cost- and time-efficient manner [1,3,4].

This study represents a preliminary investigation of the potential molecular interactions between phytochemical constituents of *B. medicinalis* and selected pro-inflammatory targets using an integrated computational approach. The aim of this study was to characterize the predicted biological and pharmacokinetic properties of the identified secondary metabolites and evaluate their potential interactions with COX-2, iNOS, TNF-α, and IL-1β using a multifaceted methodological framework, combining SAR analysis, ADME profiling, toxicity prediction, molecular docking, and molecular dynamics simulations.

Methods

Sample collection and extraction

B. medicinalis leaves were collected from the forest area of Wawopada Village, North Morowali Regency, Central Sulawesi, Indonesia. The plant material was taxonomically identified at the Plant Systematics Laboratory, Universitas Gadjah Mada, Indonesia, with voucher ID 00773/S.Tb./XI/2024. The collected leaves were washed under running tap water to remove adhering debris and air-dried at room temperature (25–30°C) for four days in a well-ventilated area protected from direct sunlight. For extraction, the dried leaves were ground into a fine powder using an electric grinder. A total of 20 g of the powder was weighed and macerated in 200 mL of absolute ethanol (≥99%) at room temperature for 24 h. The extraction comprised two consecutive 24-h maceration cycles, in which fresh solvent (150 mL) replaced the previous solvent after the first cycle. The macerates were filtered through Whatman No. 1 filter paper, and the

combined filtrates were concentrated and subsequently air-dried at room temperature until complete solvent evaporation was achieved. The resulting crude extract was stored in an airtight amber glass vial at 4°C until further analysis.

Gas chromatography-mass spectrometry (GC-MS) analysis

Gas chromatography-mass spectrometry (GC-MS) analysis was performed using a Shimadzu GCMS-QP2010 system (Shimadzu Corporation, Kyoto, Japan). A 1 µL sample was injected using the hot-needle technique at a split ratio of 49:1. Separation was performed on a 30 m Agilent DB-5MS UI column (inner diameter 0.25 mm, coating thickness 0.25 µm; Agilent Technologies, Santa Clara, CA, USA). The injector, interface, and ion source temperatures were maintained at 300°C, 30°C, and 250°C, respectively. Helium was used as the carrier gas at a constant flow rate of 0.65 mL/min.

The oven temperature program began with an initial isothermal step at 70°C for 5 min, followed by a temperature ramp of 5°C/min to 305°C. The system was then re-equilibrated at 70°C for 5 min before the next injection. Mass spectra were acquired at a rate of two scans per second over a mass range of m/z 28–600. Chromatograms and mass spectra were acquired and processed using GCMSsolution software (Shimadzu Corporation, Kyoto, Japan). Compounds were identified by comparing the acquired mass spectra with those in the NIST Mass Spectral Library on the basis of spectral similarity and retention characteristics. A similarity index (SI) of ≥80% was regarded as indicative of reliable identification.

Ligand and protein preparation

Phytochemical compounds from *B. medicinalis* were retrieved in SDF format via the PubChem database (https://pubchem.ncbi.nlm.nih.gov/). Open Babel, integrated within PyRx 0.8, was used for energy minimization using the Universal Force Field (UFF) and conjugate gradient algorithms. The ligand structures were subsequently parameterized by assigning Gasteiger charges and defining rotatable bonds before conversion to PDBQT format for flexible docking simulations [14,15]. Three-dimensional (3D) crystal structures of the target proteins were obtained from the RCSB Protein Data Bank (PDB) and prepared using BIOVIA Discovery Studio Visualizer 2025. Protein preparation involved the systematic removal of water molecules, HETATM records, and co-crystallized ligands to obtain a clean binding site for subsequent docking analysis (**Table 1**) [16].

Table 1. Protein targets involved in the inflammatory response

Protein target	PDB ID	References
Interleukin-1 beta (IL-1β)	8C3U	[12]
Cyclooxygenase-2 (COX-2)	6COX	[32]
Inducible nitric oxide synthase (iNOS)	3HR4	[33]
Tumor necrosis factor-alpha (TNF-α)	2AZ5	[34]

Prediction of biological activity and pharmacokinetic properties

The biological activity of the selected compounds was initially predicted using the Prediction of Activity Spectra for Substances (PASS) Online server. Canonical SMILES for each compound were retrieved from the PubChem database and submitted individually to the PASS Online web server. The prediction algorithm estimates the probability of specific biological activities based on SAR analysis using a large training dataset of biologically characterized compounds. The output includes the probability of activity (Pa) and the probability of inactivity (Pi) for each predicted biological effect. In this study, anti-inflammatory-related activities with Pa > Pi were considered potential predicted activities. Among these compounds, a predefined Pa threshold of >0.50 was applied to prioritize compounds for subsequent in silico analyses. Compounds meeting this threshold were selected for further analysis. This criterion was used solely for compound prioritization and was not interpreted as evidence of experimentally confirmed pharmacological activity [17,18].

Drug-likeness was subsequently evaluated using the SwissADME web server and primarily assessed according to Lipinski's Rule of Five, including molecular weight (≤500 Da), octanol/water partition coefficient (LogP≤5), hydrogen bond donors (≤5), hydrogen bond

acceptors (≤10), molar refractivity (40–130), rotatable bonds (≤10), and topological polar surface area (≤140 Å²). Compounds with no more than one Lipinski violation were considered to exhibit favorable predicted oral drug-likeness. However, these results were interpreted only as indicators of theoretical pharmacokinetic suitability and not as confirmation of oral bioavailability or clinical drug efficacy [19,20].

The toxicity profile of each selected compound was predicted using the ProTox 3.0 web server by submitting the corresponding canonical SMILES. The platform estimates acute oral toxicity (LD_{50}), toxicity class according to the Globally Harmonized System (GHS), organ toxicity, Tox21 stress response pathways, and toxicity endpoints using machine learning models trained on experimentally annotated datasets. These predictions were used to compare the relative safety profiles of the compounds and to support compound prioritization [21].

Protein-protein interaction

Target proteins (human proteins) were selected based on their biological relevance to the investigated pharmacological activity and their association with the underlying disease or inflammatory process. The resulting target list was subjected to protein–protein interaction (PPI) network analysis using STRING database v12.0 (https://string-db.org/) and applying a minimum required interaction confidence score of 0.700 to retain high-confidence protein associations. Both known and predicted interactions were considered, integrating evidence from experimental data, curated databases, co-expression, gene neighborhood, gene fusion, co-occurrence, and text-mining sources available in STRING.

Gene ontology-biological process (GO-BP) enrichment analysis (*Homo sapiens* as the reference) was performed using the functional enrichment module of STRING v12.0. Statistical significance was assessed using false discovery rate (FDR) correction with a p-value<0.05. Significant GO-BP terms were ranked based on statistical significance and the number of associated target proteins, and the enrichment results were visualized directly using the graphical visualization features of STRING v12.0. The PPI network and GO-BP enrichment analyses were subsequently used to characterize the functional relationships among the selected targets and provide a biological context for interpreting the potential mechanisms associated with the investigated compounds.

Molecular docking and analysis of protein-ligand interaction

Molecular docking simulations were performed using a site-specific docking approach implemented in the PyRx Virtual Screening Tool (v0.8) integrated with the AutoDock Vina wizard. The 3D structures of the target proteins were downloaded from the RCSB Protein Data Bank website. All chain components in the PDB file were retained in their original state to allow objective identification of the binding pockets. The active-site coordinates, including the grid box center and dimensions, were defined based on the position of the co-crystallized ligand within each protein structure (**Table 2**), thereby restricting the docking search space to the experimentally characterized binding pocket.

Table 2. Re-docking validation and grid box parameters for the protein-ligand docking simulations

PDB ID	RMSD (Å)	Grid size			Grid position (Å)			Exhaustiveness	Pose selection criteria
		X	Y	Z	X	Y	Z		
6COX	0.872	13	11	21	26.625	-4.307	26.348	10	1
3HR4	1.105	24	22	23	0.989	8.935	-65.436	10	1
2AZ5	0.602	13	16	23	-19.409	74.650	33.849	10	1
8C3U	0.580	28	28	23	-17.242	-5.454	-42.888	10	1

Re-docking was performed to verify the validity of the docking protocol. In this procedure, the co-crystallized native ligand was re-docked into the active site of each protein using the same parameters as those applied to the test compounds. The protocol was considered valid when the root-mean-square deviation (RMSD) was less than 2.0 Å [14,15,22]. RMSD values were calculated by atom-by-atom superimposition using BIOVIA Discovery Studio Visualizer (**Table 2**).

The best conformation (pose) for each protein–ligand complex was determined based on the predicted binding energy (kcal/mol), with the pose exhibiting the lowest binding energy selected for further evaluation. The selected docking poses (2D and 3D) were analyzed and visualized using BIOVIA Discovery Studio Visualizer 2025 to characterize predicted protein-ligand interactions, emphasizing hydrogen bonds and hydrophobic contacts [16].

Molecular dynamics simulation

Molecular dynamics simulations (MDS) were performed using GROMACS 2023.02 to evaluate the dynamic stability of stigmasterol in complex with the four inflammatory target proteins, namely COX-2 (6COX), iNOS (3HR4), TNF-α (2AZ5), and IL-1β (8C3U). The best-scoring docked conformation of stigmasterol with each target protein was used as the starting structure for the simulations. Each protein–ligand complex was simulated at 300 K for 100 ns. The resulting trajectories were analyzed over 0–100 ns for protein backbone root mean square deviation (RMSD), ligand RMSD, root mean square fluctuation (RMSF), protein–ligand hydrogen bonds, radius of gyration (Rg), and solvent-accessible surface area (SASA) to assess conformational stability, residue flexibility, ligand stability, intermolecular interactions, protein compactness, and solvent exposure throughout the simulation [23].

Results

Identified compounds from GC-MS

The GC–MS chromatogram of the ethanolic leaf extract of *B. medicinalis* showed multiple peaks with varying relative abundances (**Figures 1–2**). The principal compounds identified in the chromatogram included palmitic acid (11.50%), dihomo-γ-linolenic acid (10.73%), stigmasterol (7.79%), linoleic acid (5.96%), squalene (2.07%), phytol (1.87%), oleic acid (1.26%), vitamin E (0.83%), and (–)-loliolide (0.21%), with their corresponding retention times and peak areas summarized in **Table 3**.

Although Phenol, 2,4,6-tris(1,1-dimethylethyl), exhibited the highest relative abundance (29.68%), it was excluded based on the predefined selection criteria. This compound has been predominantly reported as a synthetic antioxidant used in plastics, rubber, and polymeric materials, with limited evidence supporting its pharmacological relevance as a plant-derived bioactive compound.

Structure-activity relationship (SAR) analysis

SAR-based predictions indicated anti-inflammatory activity for most of the candidate compounds, as presented in **Figure 3**. All compounds were predicted to possess anti-inflammatory potential, with Pa values ranging from 0.43 to 0.84. The predicted probability of anti-inflammatory activity varied widely, from comparatively low values for heptadecane (43%) to higher values for 9,12-hexadecadienoic acid methyl ester, 9,12-octadecadienoic acid (Z,Z)-(linoleic acid), and dihomo-γ-linolenic acid (75%); vitamin E (83%); and 9,12,15-octadecatrien-1-ol (84%).

Table 3. GC–MS identification of selected compounds in the ethanolic extract of *B. medicinalis*

Compound name	Compound ID	Molecular formula	Retention time (min)	Area (%)	Similarity index (%)
L-limonene	439250	$C_{10}H_{16}$	9.542	0.43	96
Nonanoic acid	8158	$C_9H_{18}O_2$	23.908	0.43	79
Heptadecane	12398	$C_{17}H_{36}$	24.111	0.24	93
1-Nonadecene	29075	$C_{19}H_{38}$	24.518	0.21	85
Tetradecanoic acid	11005	$C_{14}H_{28}O_2$	30.423	0.62	90
(-)-Loliolide	100332	$C_{11}H_{16}O_3$	30.883	0.21	82
1-Heptacosanol	74822	$C_{27}H_{56}O$	31.144	0.15	82
9-Eicosyne	557019	$C_{20}H_{38}$	32.745	2.48	88
Methyl palmitate	8181	$C_{17}H_{34}O_2$	34.104	0.77	97
Palmitic acid	985	$C_{16}H_{32}O_2$	34.842	11.50	95
Ethyl palmitate	12366	$C_{18}H_{36}O_2$	35.514	0.44	93
Eugenyl acetate	136	$C_{12}H_{14}O_3$	36.892	0.21	55
9,12-Hexadecadienoic acid, methyl ester	549033	$C_{17}H_{30}O_2$	37.511	0.44	93

Compound name	Compound ID	Molecular formula	Retention time (min)	Area (%)	Similarity index (%)
Phytol	5280435	$C_{20}H_{40}O$	37.991	1.67	95
9,12-Octadecadienoic acid (Z,Z)- / Linoleic acid	5280450	$C_{18}H_{32}O_2$	38.249	5.96	92
Dihomo-γ-linolenic acid	5280581	$C_{20}H_{34}O_2$	38.376	10.73	87
Oleic acid	445639	$C_{18}H_{34}O_2$	38.804	1.26	91
9,12,15-Octadecatrien-1-ol	68169	$C_{18}H_{32}O$	38.919	0.45	88
Squalene	638072	$C_{30}H_{50}$	49.704	2.07	95
Vitamin E	14985	$C_{29}H_{50}O_2$	55.185	0.83	84
Stigmasterol	5280794	$C_{29}H_{48}O$	57.075	7.79	91

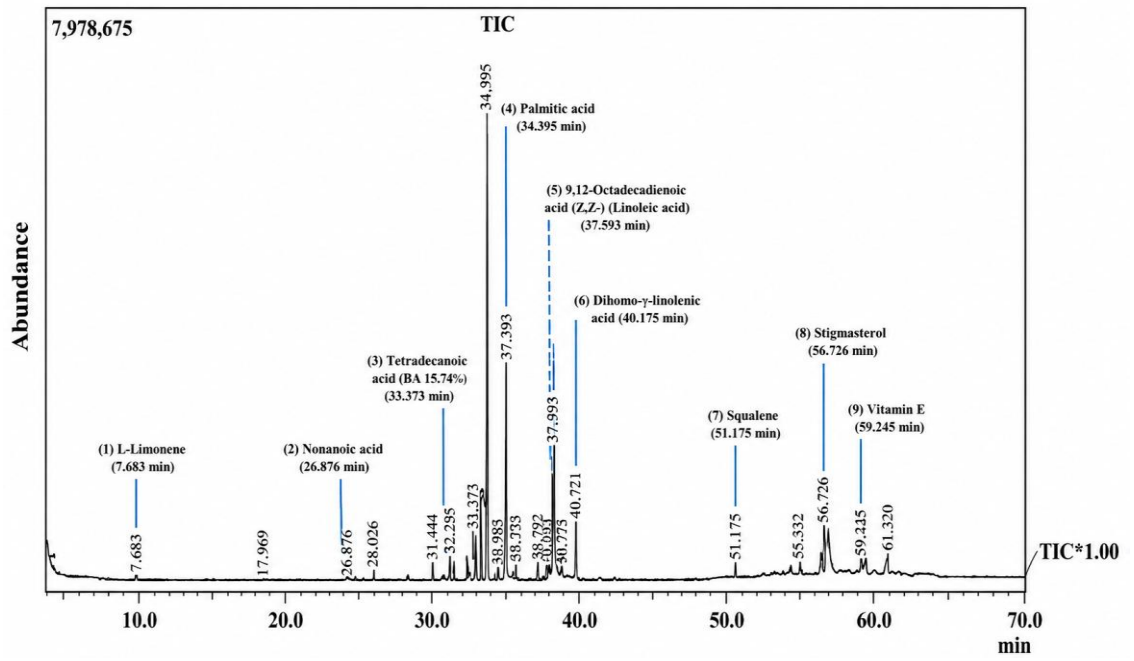

Figure 1. GC-MS chromatogram of the ethanolic extract of *B. medicinalis* leaves showing the identified compounds. Selected chromatographic peaks are labeled according to their GC-MS library matches.

Pharmacokinetic analysis

Among the 21 compounds identified by GC-MS, 17 compounds met the predefined Pa threshold of >0.50 for anti-inflammatory-related activity and were therefore selected for subsequent pharmacokinetic and drug-likeness analyses. The drug-likeness analysis showed that all evaluated compounds had molecular weight (MW) below 500 Da (range, 136.23–430.71 Da), 0–1 hydrogen bond donors (HBD), and 0–3 hydrogen bond acceptors (HBA), thereby satisfying the Lipinski criteria for these three parameters. The cLogP values range from 1.55 to 8.29. Five compounds—L-limonene, nonanoic acid, tetradecanoic acid, (-)-loliolide, and eugenyl acetate—had cLogP values ≤5, whereas the remaining 12 compounds had cLogP values >5. Molar refractivity (MR) values ranged from 47.12 to 143.48, the number of rotatable bonds (n-ROTB) ranged from 0 to 16, and the topological polar surface area (TPSA) ranged from 0.00 to 46.53 Å^2. Based on Lipinski's Rule of Five, five compounds satisfied all evaluated criteria, while the remaining 12 compounds had a single violation related to cLogP, with no violations of the MW, HBD, or HBA criteria (**Table 4**).

Toxicity analysis

Toxicity predictions covered LD_{50} values, toxicity classes, organ toxicity, Tox21 stress response pathways, and toxicity endpoints (**Figure 4A-E**). Predicted LD_{50} values varied substantially among the 17 compounds, ranging from 10 to 5,000 mg/kg (**Figure 4A**). Methyl palmitate, ethyl palmitate, squalene, and vitamin E showed the highest predicted LD_{50} values (5,000 mg/kg), followed by L-limonene (4,400 mg/kg), eugenyl acetate (1,670 mg/kg), stigmasterol (890 mg/kg), nonanoic acid and tetradecanoic acid (900 mg/kg each), palmitic acid (900 mg/kg), 9-eicosyne (300 mg/kg), oleic acid (48 mg/kg), and (–)-loliolide (34 mg/kg).

Permatasari et al. Narra X 2026; 4 (2): e303 - http://doi.org/10.52225/narrax.v4i2.303

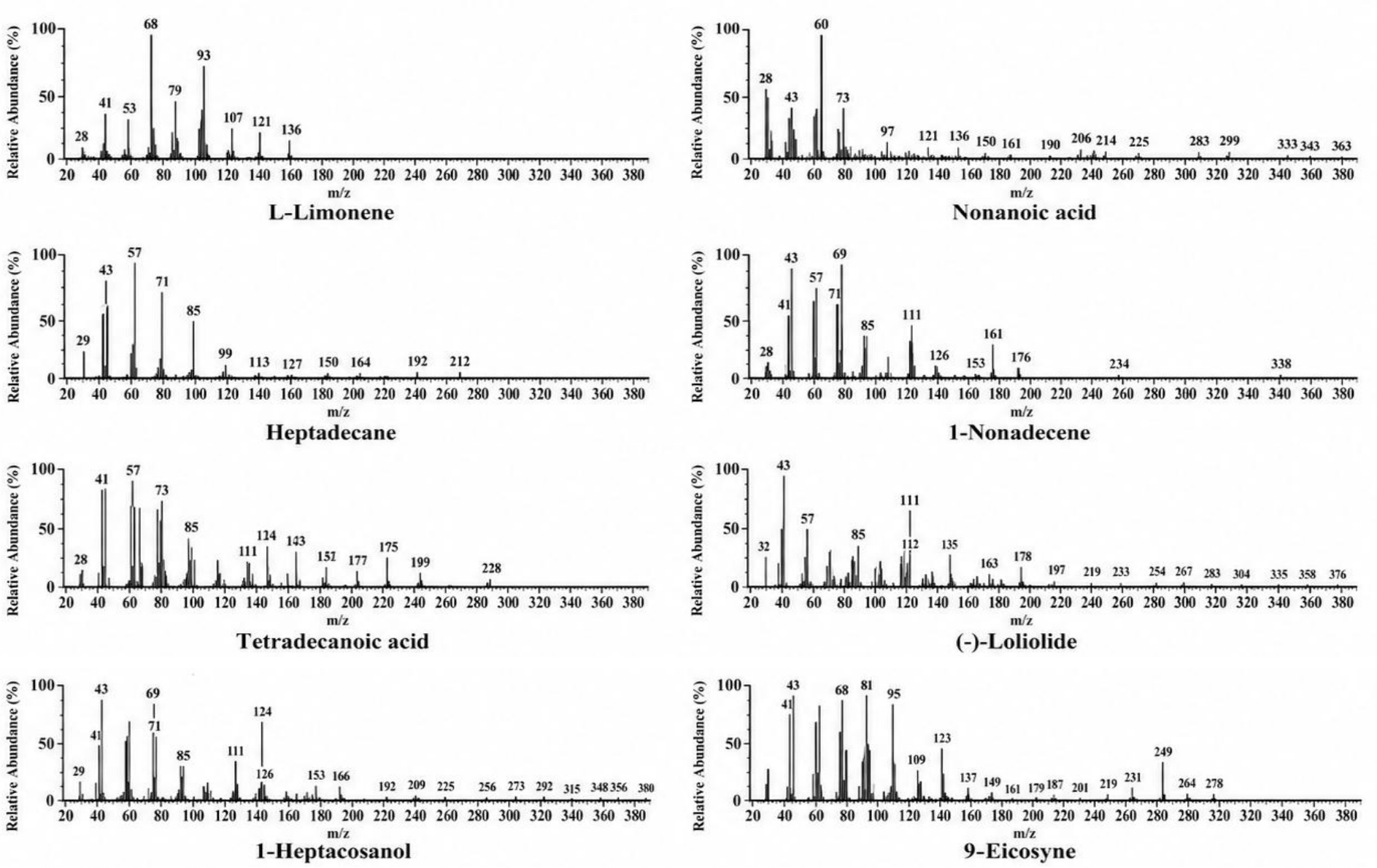

Figure 2. GC–MS mass spectra of the selected compounds identified in the ethanolic extract of *B. medicinalis* leaves. The selected compound identification was achieved through comparison of the obtained mass spectra with the NIST mass spectral database using characteristic fragmentation patterns, percent concentration, and acceptable similarity index (SI) values.

Permatasari et al. Narra X 2026; 4 (2): e303 - http://doi.org/10.52225/narrax.v4i2.303

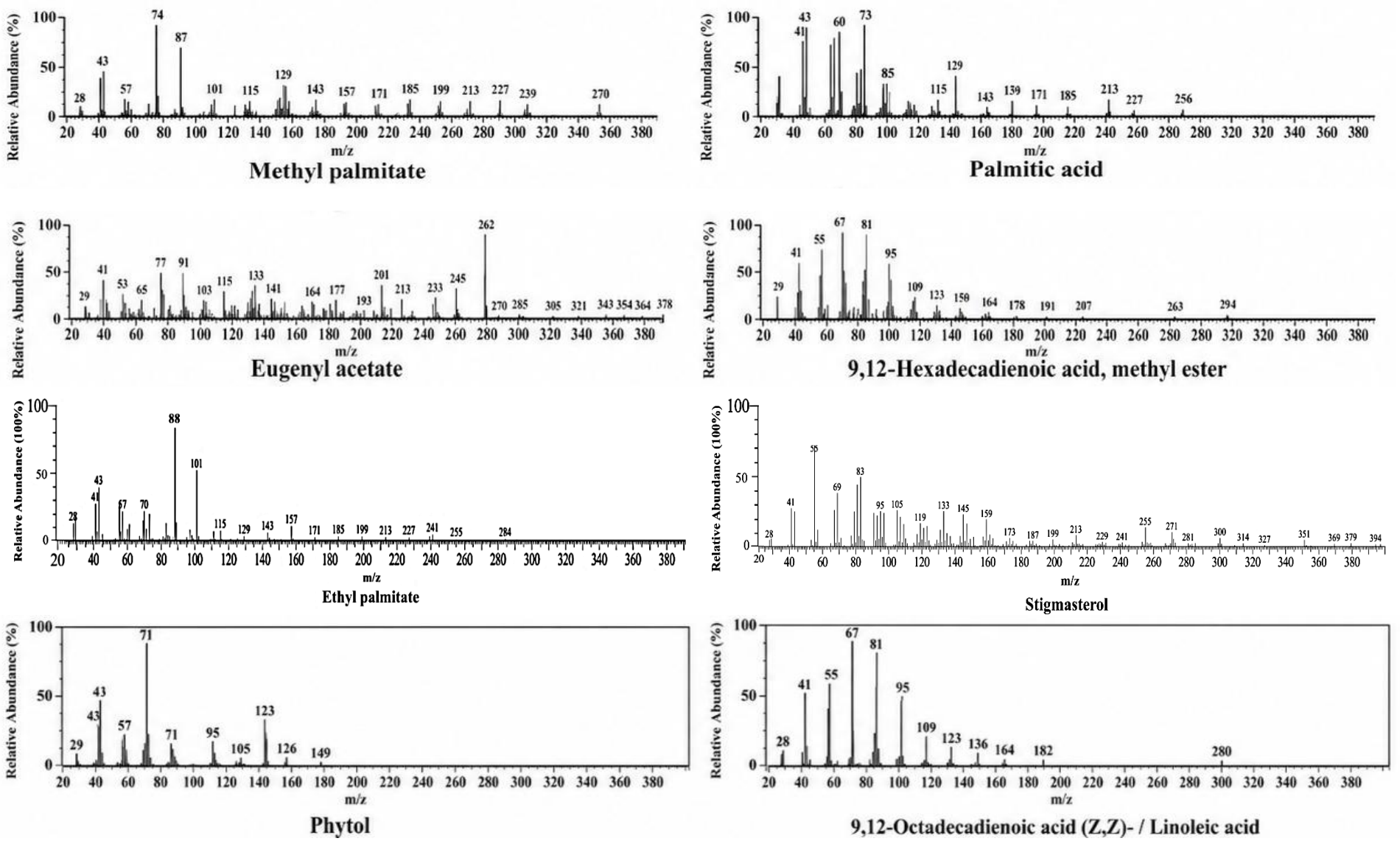

Figure 2 (continued). GC–MS mass spectra of the selected compounds identified in the ethanolic extract of *B. medicinalis* leaves. The selected compound identification was achieved through comparison of the obtained mass spectra with the NIST mass spectral database using characteristic fragmentation patterns, percent concentration, and acceptable similarity index (SI) values.

Permatasari et al. Narra X 2026; 4 (2): e303 - http://doi.org/10.52225/narrax.v4i2.303

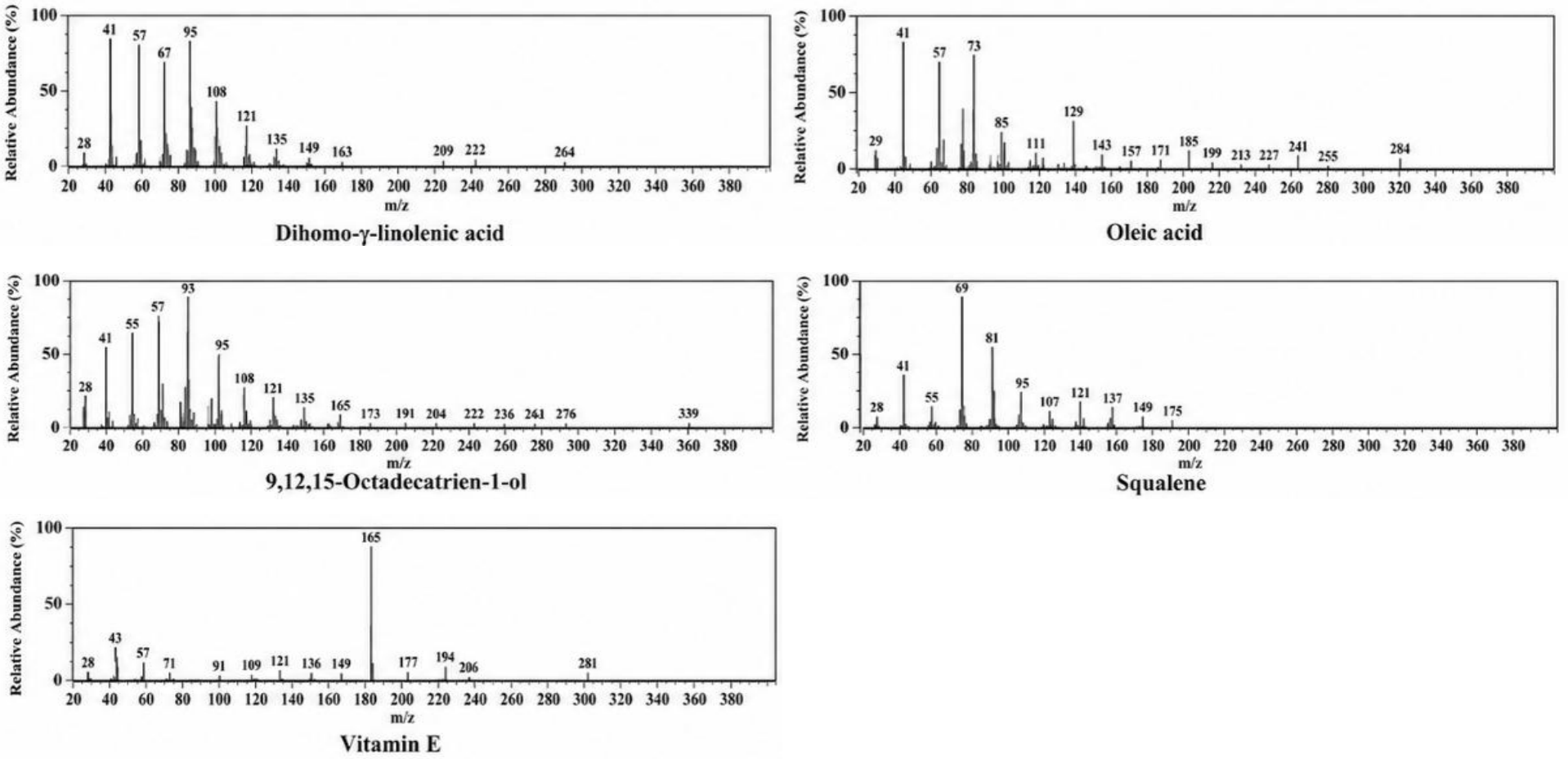

Figure 2 (continued). GC–MS mass spectra of the selected compounds identified in the ethanolic extract of *B. medicinalis* leaves. The selected compound identification was achieved through comparison of the obtained mass spectra with the NIST mass spectral database using characteristic fragmentation patterns, percent concentration, and acceptable similarity index (SI) values.

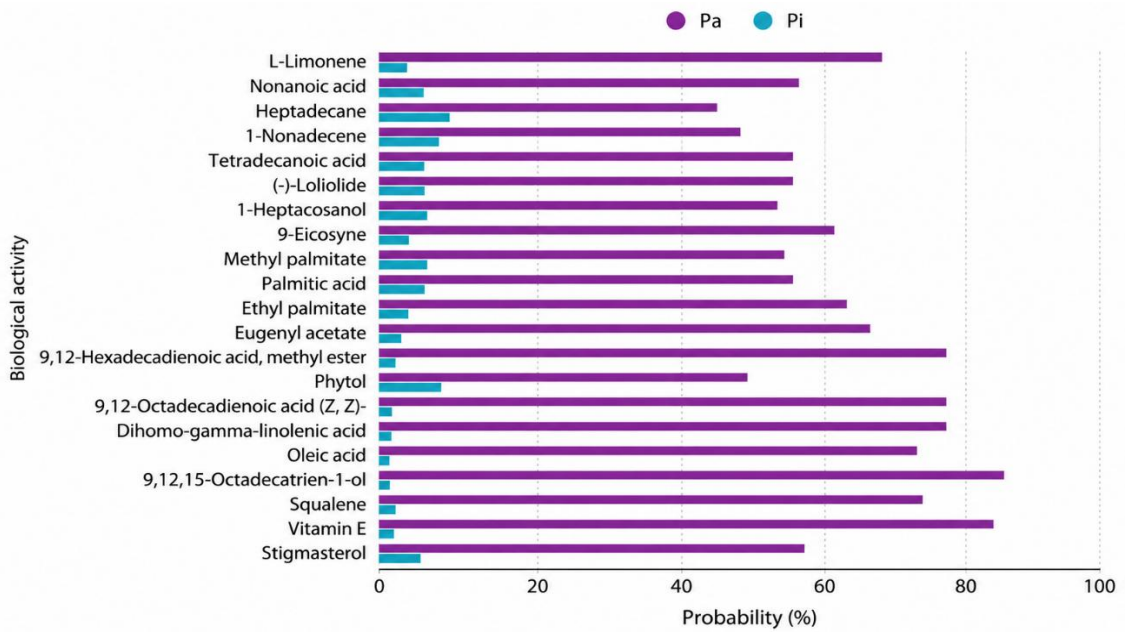

Figure 3. Predicted anti-inflammatory activity of compounds identified in the ethanolic extract of *B. medicinalis* leaves using the PASS Online web server. Probability of activity (Pa) represents the predicted probability that a compound exhibits anti-inflammatory activity, whereas probability of inactivity (Pi) represents the predicted probability that the compound does not exhibit the activity.

Table 4. Predicted physicochemical and drug-likeness properties of compounds identified in the ethanolic extract of *B. medicinalis* leaves

Compound name	MW (≤500)	HBD (≤5)	HBA (≤10)	cLogP (≤5)	MR (40–130)	n-ROTB (≤10)	TPSA (Å²)
L-limonene	136.23	0	0	3.35	47.12	1	0.00
Nonanoic acid	158.24	1	2	2.60	47.15	7	37.30
Tetradecanoic acid	228.37	1	2	4.45	71.18	12	37.30
(-)-Loliolide	196.24	1	3	1.55	52.51	0	46.53
9-Eicosyne	278.52	0	0	7.51	96.42	14	0.00
Methyl palmitate	270.45	0	2	5.54	85.12	15	26.30
Palmitic acid	256.42	1	2	5.20	80.80	14	37.30
Ethyl palmitate	284.48	0	2	5.90	89.92	16	26.30
Eugenyl acetate	206.24	0	3	2.55	58.54	5	35.53
9,12-Hexadecadienoic acid, methyl ester	266.42	0	2	5.05	84.17	13	26.30
9,12-Octadecadienoic acid (Z,Z)-	280.45	1	2	6.25	89.46	14	37.30
Dihomo-γ-linolenic acid	306.48	1	2	6.25	98.60	15	37.30
Oleic acid	282.46	1	2	5.65	89.94	15	37.30
9,12,15-Octadecatrien-1-ol	264.45	1	1	5.50	88.38	13	20.23
Squalene	410.72	0	0	6.25	143.48	15	0.00
Vitamin E	430.71	1	2	8.29	139.27	12	29.46
Stigmasterol	412.69	1	1	6.98	132.75	5	20.23

cLogP: calculated logarithm of the partition coefficient; HBA: hydrogen bond acceptors; HBD: hydrogen bond donors; MR: molar refractivity; MW: molecular weight; n-RotB: number of rotatable bonds; TPSA: topological polar surface area

The lowest predicted LD_{50} values were observed for 9,12-octadecadienoic acid (Z,Z) and dihomo-γ-linolenic acid (10 mg/kg each), followed by 9,12-hexadecadienoic acid, methyl ester (20 mg/kg) and 9,12,15-octadecatrien-1-ol (11.73 mg/kg). The predicted toxicity classes ranged from Class 2 to Class 6 (**Figure 4B**). Organ toxicity analysis indicated that most compounds were predicted to be inactive for the evaluated endpoints, while selected compounds showed positive predictions for specific organ toxicity parameters (**Figure 4C**). The Tox21 analysis of stress responses demonstrated that the majority of compounds were classified as inactive across the assessed pathways, with only a limited number of compounds exhibiting positive predictions for individual stress-response pathways (**Figure 4D**). Similarly, the toxicity endpoint analysis

showed that most compounds were predicted to be inactive for the evaluated toxicity endpoints, whereas positive predictions were observed only for specific compounds and endpoints (**Figure 4E**).

Protein-protein interaction (PPI)

PPI prediction displays the interaction networks of four selected inflammatory targets (COX-2, iNOS, TNF-α, and IL-1β), as presented in **Figures 5A-D**. The COX-2 network consisted of 29 nodes (**Figure 5A**), whereas the iNOS network comprised 37 nodes (**Figure 5B**). Among the analyzed targets, the TNF-α network displayed the greatest complexity, containing 48 protein nodes (**Figure 5C**), and the IL-1β network contained 95 nodes (**Figure 5D**). In all four networks, edge thickness reflects the confidence level of the interactions, which is derived from a combination of experimental data, curated databases, gene co-expression, and text mining.

Biological process (BP)

Biological process (BP) enrichment analysis of the target proteins (COX-2, iNOS, TNF-α, and IL-1β) is summarized in **Figure 6A-D**. The most significantly enriched GO-BP terms were selected for presentation based on the predefined enrichment criteria. COX-2 was enriched in the cyclooxygenase pathway, prostaglandin biosynthetic process, prostaglandin metabolic process, arachidonic acid metabolic process, eicosanoid biosynthetic process, and metabolic processes (**Figure 6A**). iNOS was associated with regulation of nitric oxide synthase activity, positive regulation of nitric oxide synthase activity, regulation of nitric oxide biosynthetic process, positive regulation of nitric oxide biosynthetic process, positive regulation of monooxygenase activity, negative regulation of nitric oxide synthase activity, and negative regulation of oxidoreductase activity (**Figure 6B**). TNF-α showed enrichment in the tumor necrosis factor-mediated signaling pathway, positive regulation of NF-κB transcription factor activity, regulation of IκB kinase/NF-κB signaling, positive regulation of IκB kinase/NF-κB signaling, IκB kinase/NF-κB signaling, positive regulation of the JNK cascade, TNFSF11-mediated signaling pathway, and apoptotic signaling pathway (**Figure 6C**).

IL-1β was enriched in regulation of interleukin-1 beta production, positive regulation of interleukin-1 beta production, positive regulation of cytokine production, negative regulation of interleukin-1 beta production, negative regulation of interleukin-1 production, regulation of tumor necrosis factor production, positive regulation of tumor necrosis factor production, regulation of interleukin-8 production, positive regulation of interleukin-6 production, and negative regulation of cytokine production (**Figure 6D**).

Molecular docking

Among the 17 identified compounds, 10 compounds were prioritized for further molecular docking analysis based on the integration of several in silico parameters, including predicted biological activity with Pa greater than Pi, favorable pharmacokinetic profiles, and acceptable toxicity predictions. Molecular docking analysis revealed that the 10 selected compounds exhibited varying predicted binding affinities toward the four inflammation-related targets (COX-2, iNOS, TNF-α, and IL-1β), with binding energies ranging from −4.7 to −8.6 kcal/mol. Among the tested compounds, stigmasterol showed the most favorable predicted binding energies toward COX-2 (−8.6 kcal/mol) and TNF-α (−8.4 kcal/mol), whereas squalene displayed relatively favorable binding toward COX-2 (−8.1 kcal/mol). Vitamin E exhibited comparable predicted binding affinities toward iNOS and IL-1β (−7.7 kcal/mol for both targets; **Table 5**).

Molecular interaction mapping

Interaction analysis of the top-scoring docked compound (stigmasterol) is summarized in **Table 6**. In the COX-2 complex, stigmasterol interacted with HIS388, VAL444, ALA443, LEU408, LEU391, LEU390, and ALA199 in chain A, with interaction distances ranging from 3.94 to 5.43 Å.

Permatasari et al. Narra X 2026; 4 (2): e303 - http://doi.org/10.52225/narrax.v4i2.303

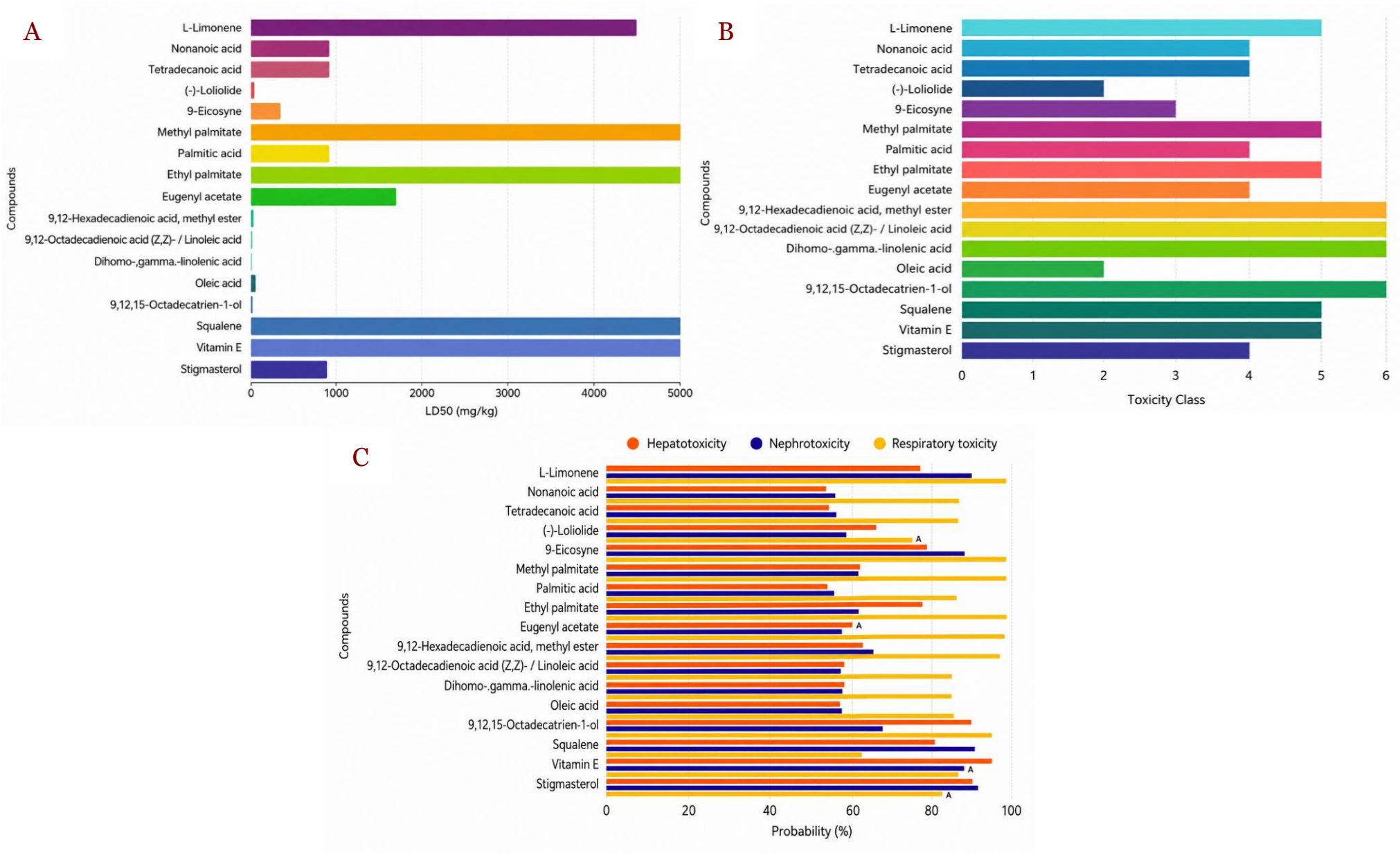

Figure 4. Predicted toxicity profiles obtained using ProTox 3.0. (A) Lethal dose 50% (LD_{50}), (B) toxicity class, and (C) organ toxicity.

Permatasari et al. Narra X 2026; 4 (2): e303 - http://doi.org/10.52225/narrax.v4i2.303

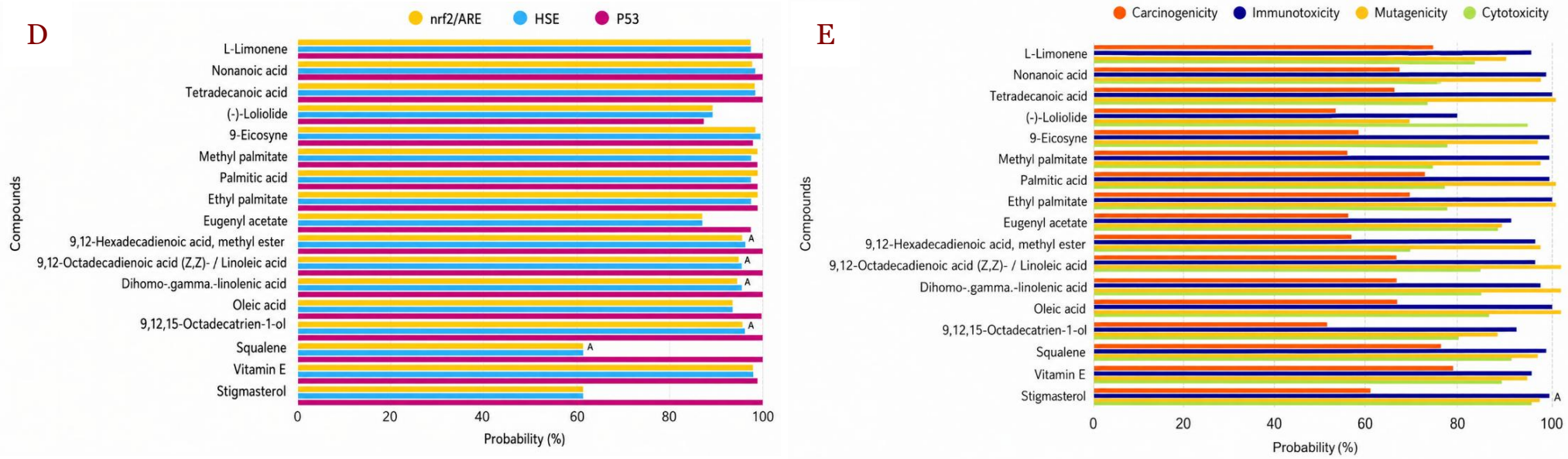

Figure 4 (continued). Predicted toxicity profiles obtained using ProTox 3.0. (D) Tox21 stress response pathways and (E) toxicity endpoints.

Permatasari et al. Narra X 2026; 4 (2): e303 - http://doi.org/10.52225/narrax.v4i2.303

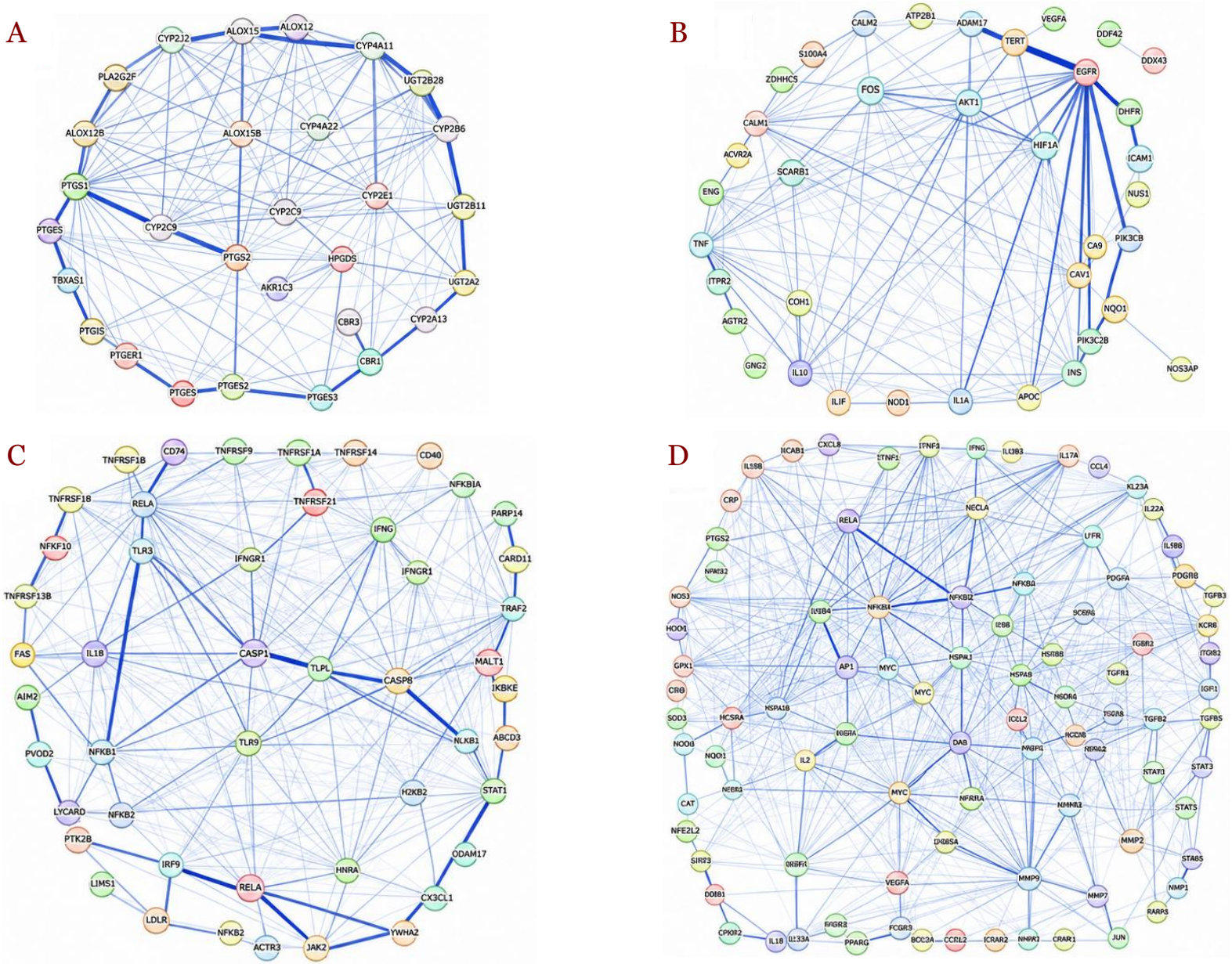

Figure 5. Protein-protein interaction (PPI) networks of the target proteins and their functional partners. (A) COX-2, (B) iNOS, (C) TNF-α, and (D) IL-1β. Larger nodes indicate higher network connectivity, while thicker and darker edges indicate higher interaction confidence.

Permatasari et al. Narra X 2026; 4 (2): e303 - http://doi.org/10.52225/narrax.v4i2.303

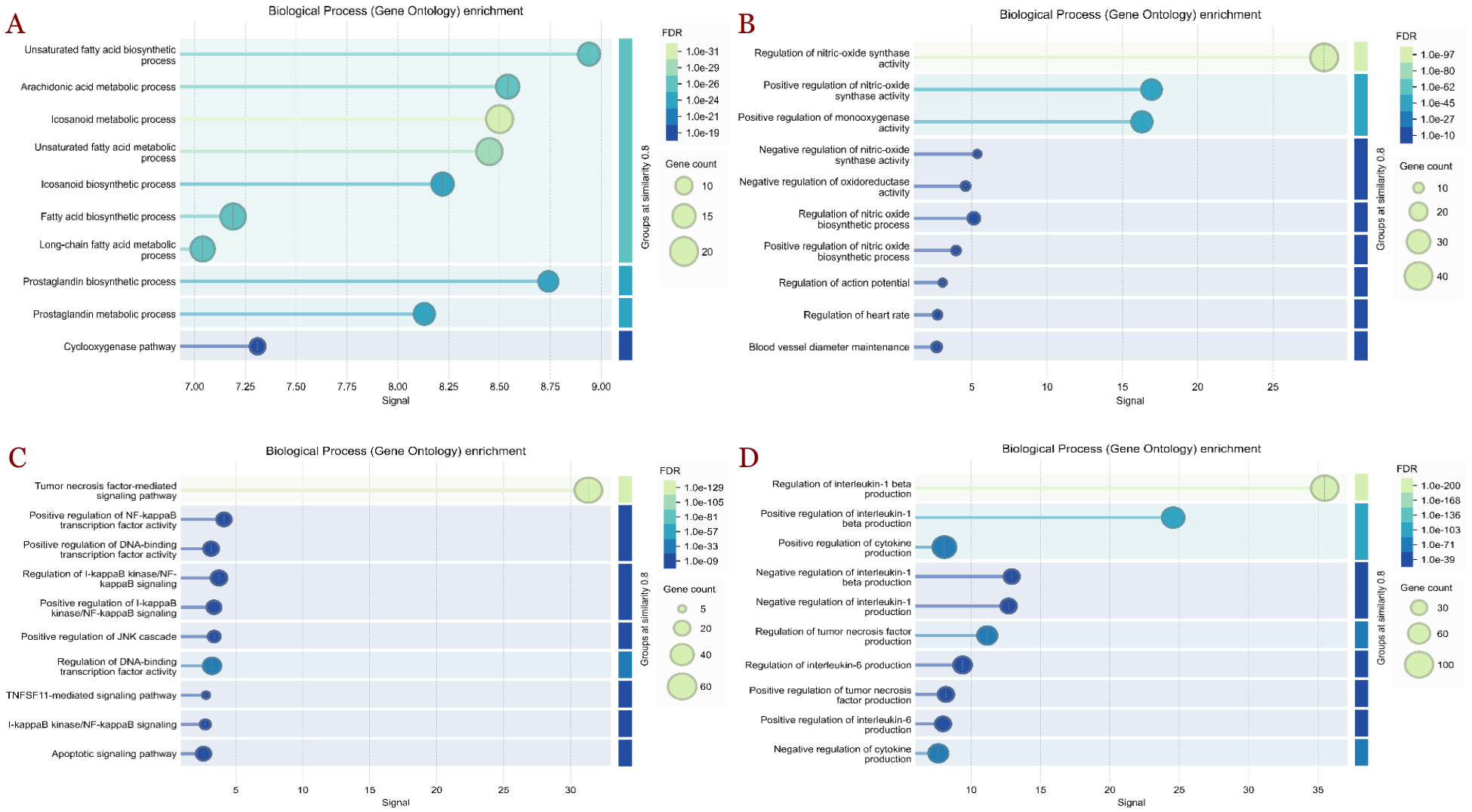

Figure 6. Enriched biological processes (BP) associated with the four target proteins. (A) COX-2, (B) iNOS, (C) TNF-α, and (D) IL-1β.

Table 5. Predicted binding affinities of the selected compounds against the four target proteins (COX-2, iNOS, TNF-α, and IL-1β)

Ligand	Binding energy (kcal/mol)			
	COX-2	iNOS	TNF-α	IL-1β
L-limonene	−6.0	−6.5	−5.5	−5.7
Nonanoic acid	−5.5	−5.8	−4.7	−4.9
Tetradecanoic acid	−6.2	−6.1	−4.8	−5.6
Methyl palmitate	−6.5	−5.5	−5.3	−5.8
Palmitic acid	−6.5	−6.4	−5.4	−5.8
Ethyl palmitate	−6.2	−5.8	−5.3	−5.4
Eugenyl acetate	−6.6	−7.1	−5.9	−5.9
Squalene	−8.1	−6.9	−7.3	−7.2
Vitamin E	−7.9	−7.7	−7.6	−7.7
Stigmasterol	−8.6	−7.7	−8.4	−7.7

For iNOS, the key predicted contacts involved TYR631 and PHE593 in chain A, with distances ranging from 3.86 to 4.47 Å. In the TNF-α complex, stigmasterol interacted with LEU55 in chain D, with an interaction distance of 5.27 Å.

For IL-1β, stigmasterol interacted with the A chain via residues VAL47, LYS97, VAL100, PRO57, PRO23, and ALA115, with distances ranging from 3.99 to 4.89 Å. All the interactions identified were hydrophobic in nature. The detailed interactions between stigmasterol and the four target proteins are visualized in **Figure 7**.

Table 6. Molecular interactions of stigmasterol with COX-2, iNOS, TNF-α, and IL-1β

Protein	Binding energy (kcal/mol)	Interacting residues	Distance (Å)	Category	Type
COX-2	-8.6	HIS388 (A)	4.22	Hydrophobic	Pi-Alkyl
		VAL444 (A)	4.96 and 5.38	Hydrophobic	Alkyl
		ALA443 (A)	5.43	Hydrophobic	Alkyl
		LEU408 (A)	4.89	Hydrophobic	Alkyl
		LEU391 (A)	4.06 and 5.37	Hydrophobic	Alkyl
		LEU390 (A)	4.34	Hydrophobic	Alkyl
		ALA199 (A)	3.94	Hydrophobic	Alkyl
iNOS	-7.7	TYR631 (A)	3.86 and 4.47	Hydrophobic	Pi-Alkyl
		PHE593 (A)	4.29	Hydrophobic	Pi-Alkyl
TNF-α	-8.4	LEU55 (D)	5.27	Hydrophobic	Alkyl
IL-1β	-7.7	VAL47 (A)	4.56 and 4.89	Hydrophobic	Alkyl
		LYS97 (A)	3.99	Hydrophobic	Alkyl
		VAL100 (A)	4.77 and 4.82	Hydrophobic	Alkyl
		PRO57 (A)	4.21	Hydrophobic	Alkyl
		PRO23 (A)	4.49	Hydrophobic	Alkyl
		ALA115 (A)	4.39 and 4.83	Hydrophobic	Alkyl

Molecular dynamics simulation

MDS were performed for 100 ns to evaluate the dynamic stability of stigmasterol in complex with COX-2, TNF-α, IL-1β, and iNOS (**Figure 8**). The average backbone RMSD values were 2.751±0.004 Å, 2.073±0.002 Å, 2.220±0.005 Å, and 3.321±0.013 Å for COX-2, TNF-α, IL-1β, and iNOS, respectively (**Figure 8A**). Meanwhile, stigmasterol showed relatively low ligand RMSD values across all complexes, with averages of 1.636±0.003 Å for COX-2, 1.393±0.004 Å for TNF-α, 1.406±0.003 Å for IL-1β, and 1.320±0.004 Å for iNOS (**Figure 8B**).

RMSF analysis showed average fluctuations of 1.270±0.513 Å, 1.029±0.509 Å, 1.355±0.850 Å, and 2.168±1.137 Å for COX-2, TNF-α, IL-1β, and iNOS, respectively (**Figure 8C**). Protein–ligand hydrogen-bond analysis showed average numbers of 0.017±0.002, 0.339±0.007, 0.609±0.009, and 0.076±0.003 for COX-2, TNF-α, IL-1β, and iNOS, corresponding to occupancies of 1.100%, 25.388%, 37.866%, and 5.649%, respectively (**Figure 8D**). The average Rg values were 24.604±0.001 Å for COX-2, 15.183±0.001 Å for TNF-α, 14.733±0.001 Å for IL-1β, and 19.341±0.006 Å for iNOS, with relatively limited variations throughout the simulation (**Figure 8E**). SASA trajectories also showed relatively consistent profiles throughout the simulation period (**Figure 8F**). Overall, the MD trajectories indicated that stigmasterol remained associated with the four target proteins during the 100-ns simulations.

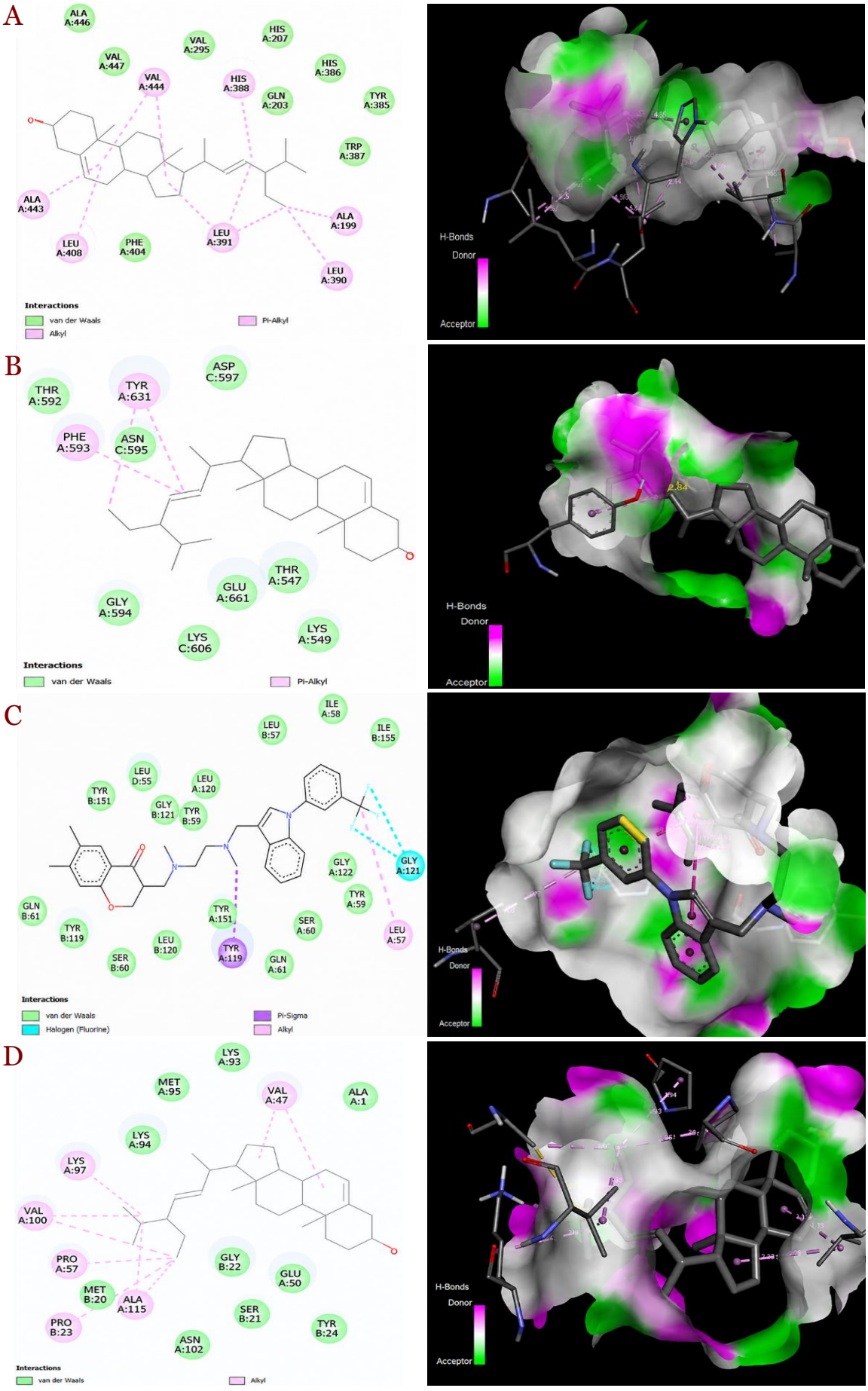

Figure 7. Two- and three-dimensional docked poses of stigmasterol with (A) COX-2 (6COX), (B) iNOS (3HR4), (C) TNF-α (2AZ5), and (D) IL-1β (8C3U).

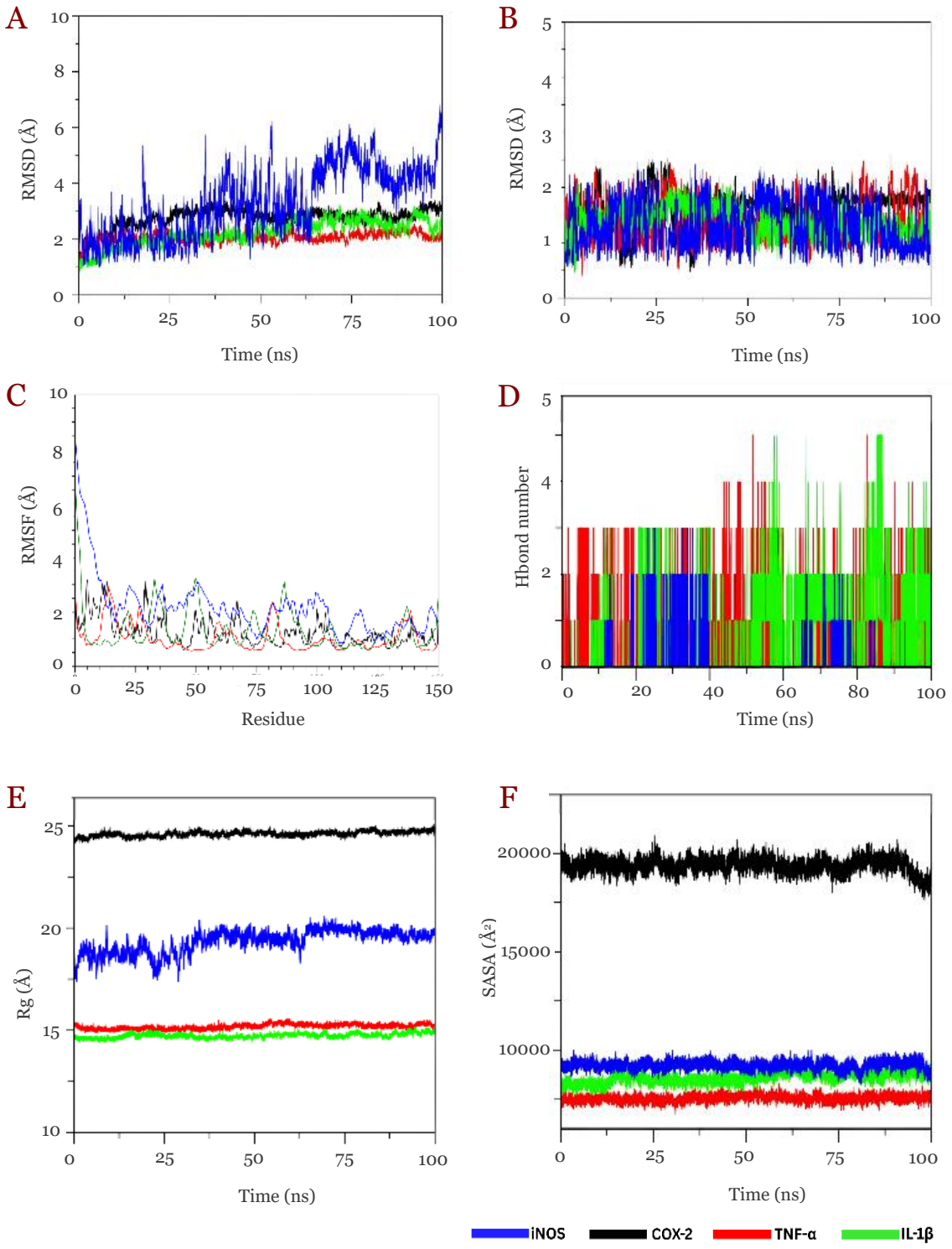

Figure 8. Molecular dynamics simulation (MDS) analyses of stigmasterol complexes with COX-2, TNF-α, IL-1β, and iNOS over 100 ns. (A) Backbone RMSD, (B) ligand RMSD, (C) RMSF, (D) hydrogen bonds, (E) radius of gyration (Rg), and (F) solvent-accessible surface area (SASA).

Discussion

B. medicinalis exhibits a broad spectrum of pharmacological activities, including antioxidant, antiviral, anticancer, antibacterial, and immunomodulatory effects [8,10,24]. The present study confirmed the presence of various lipid-related constituents, particularly terpenoids, vitamins, and steroids, in the ethanol extract of *B. medicinalis* leaves, which aligns with previous reports [8,24]. The identification of key constituents such as squalene (triterpenoid), vitamin E, and stigmasterol (steroid) underscores the therapeutic versatility of this extract, as these compounds

have been documented to possess anti-inflammatory, anticancer, antioxidant, and neuroprotective properties, among others [9,25-30].

Following the phytochemical profiling, this research proceeded with computational analysis, including SAR analysis, ADME, and toxicity assessments, PPI analysis, biological process evaluation, and molecular docking to assess the feasibility profile of selected compounds and their interactions with target proteins associated with specific activities. SAR predictions indicated anti-inflammatory activity for all compounds, albeit with variable Pa values. The ADME assessment demonstrated adherence to Lipinski's rule of five, with a single violation of the cLogP parameter; such a deviation remains acceptable, as many approved therapeutics display one violation while retaining favorable oral bioavailability [19]. Meanwhile, toxicity analysis revealed that each selected compound displayed varying values for LD_{50}, toxicity class, organ toxicity, Tox21 stress response pathways, and toxicity endpoints [21].

Furthermore, the PPI and GO-BP analyses revealed that the target proteins (COX-2, iNOS, TNF-α, and IL-1β) interact with a range of proteins involved in the inflammatory process. Docking simulations identified stigmasterol as the most promising lead candidate, exhibiting the most favorable predicted binding across the four targets: COX-2 (−8.6 kcal/mol), TNF-α (−8.4 kcal/mol), iNOS (−7.7 kcal/mol), and IL-1β (−7.7 kcal/mol). This predicted affinity provides a plausible molecular rationale for the anti-inflammatory potential of this Sulawesi-endemic species. Interaction mapping indicated that the predicted stability of the stigmasterol-protein complexes is governed mainly by hydrophobic interactions with key residues within the binding pocket of each target [31,33].

These observations are consistent with previous evidence that stigmasterol modulates inflammatory responses by suppressing pro-inflammatory mediators such as IL-1 and IL-6 [29,31]. These findings have important implications for the development of phytopharmaceuticals derived from Sulawesi's biodiversity and provide preliminary computational support for the traditional use of *B. medicinalis* by local communities. By targeting multiple inflammatory pathways simultaneously (a multi-target approach), *B. medicinalis* extract may have the potential to be developed into a therapeutic agent with a more favorable safety profile than conventional anti-inflammatory drugs such as NSAIDs, which are frequently associated with gastrointestinal and renal adverse effects during long-term use.

The MD simulations further supported the docking results by demonstrating relatively stable stigmasterol–protein complexes throughout the 100-ns trajectories. In particular, the relatively low ligand RMSD values (1.320–1.636 Å) indicated limited displacement of stigmasterol within the protein-binding environment.

The COX-2–stigmasterol complex showed an average RMSF of 1.270±0.513 Å and an Rg of 24.604±0.001 Å, which are comparable with previous findings [35], where an average RMSF of 1.11±0.53 Å and Rg of 24.05±0.07 Å were observed for a COX-2–stigmasterol complex, supporting stable conformational behavior of this interaction [35]. Similarly, Rahman *et al.* reported that stigmasterol remained stable during MD simulation with an average ligand RMSD of 1.35±0.25 Å, which is within the range observed for stigmasterol in the present study [36].

Although hydrogen-bond occupancy varied considerably among the four targets, this does not necessarily indicate weak complex stability because the docking analysis showed that stigmasterol binding was predominantly mediated by hydrophobic interactions. Collectively, the MD results complement the docking predictions and further support stigmasterol as a candidate capable of maintaining interactions with multiple inflammation-related targets.

Despite providing a comprehensive computational assessment, this study has several limitations. The biological activities indicated by PASS analysis, target prediction, network pharmacology, and molecular docking are preliminary computational data and should not be regarded as definitive proof of pharmacological activity. Furthermore, molecular dynamics simulations were performed only for the stigmasterol–protein complexes; therefore, the dynamic stability of the complexes formed by the other docked compounds was not evaluated. In addition, the computational predictions were not supported by experimental validation (in vitro and in vivo) to confirm the anti-inflammatory effects and clarify the underlying molecular mechanisms responsible for the potential therapeutic effects of stigmasterol and the total extract of *B.*

medicinalis. As a result, the current findings should be viewed as hypothesis-generating, laying the groundwork for future computational and experimental research.

Conclusion

This study indicates that the ethanol extract of *B. medicinalis* leaves contains diverse secondary metabolites, including terpenoids, vitamins, and steroids. Integrated in silico analyses predicted that several of these constituents possess anti-inflammatory potential, favorable drug-likeness profiles, and acceptable predicted safety profiles. Molecular docking predicted that stigmasterol has the most favorable binding affinity toward each protein target, with the predicted interactions predominantly involving hydrophobic contacts. MD simulations further indicated that the stigmasterol–target complexes maintained dynamic stability throughout the 100-ns simulations based on the evaluated structural and interaction parameters. These findings are consistent with the traditional use of *B. medicinalis* as an anti-inflammatory remedy and support further investigation of stigmasterol as a candidate compound. Collectively, these computational findings provide a preliminary molecular basis for further investigation of *B. medicinalis* and its constituents as potential anti-inflammatory candidates. However, the findings remain predictive and require experimental validation through in vitro and in vivo studies before their pharmacological relevance can be established.

Ethics approval

None to declare.

Acknowledgments

The authors gratefully acknowledge the Indonesia Endowment Fund for Education (Lembaga Pengelola Dana Pendidikan) under the Ministry of Finance of the Republic of Indonesia for the financial support provided for this research.

Competing interests

All authors declare that they have no conflicts of interest.

Funding

This work was supported by the Indonesia Endowment Fund for Education (Lembaga Pengelola Dana Pendidikan, LPDP), Ministry of Finance of the Republic of Indonesia, under Grant 20230621198481.

Underlying data

Supplementary material is available from the corresponding author on request.

Declaration of artificial intelligence use

An AI-assisted tool (ChatGPT) was used exclusively to support language editing during manuscript preparation. The authors carefully reviewed and approved all content and take full responsibility for the final manuscript. All of the authors maintain full responsibility for all interpretations and conclusions drawn in this study.

How to cite

Permatasari NKD, Wahyuningsih S, Podhi FM, *et al*. In silico screening of potential anti-inflammatory compounds from Sulawesi-endemic *Begonia medicinalis*. Narra X 2026; 4 (2): e303 - http://doi.org/10.52225/narrax.v4i2.303.

References

1. Enni MA, Maraj MAA. In silico drug repurposing for inflammatory diseases: A systematic review of molecular docking and virtual screening studies. Am J Adv Technol Eng Solut 2022;02(04):35-64.

2. Nayak A, Gadnayak A, Dash KT, *et al*. Exploring molecular docking with MM-GBSA and molecular dynamics simulation to predict potent inhibitors of cyclooxygenase (COX-2) enzyme from terpenoid-based active principles of Zingiber species. J Biomol Struct Dyn 2023;41(20):10840-10850.
3. Ali A, Wani AB, Malla BA, *et al*. Network pharmacology integrated molecular docking and dynamics to elucidate saffron compounds targeting human COX-2 protein. Medicina 2023;59(12):2058.
4. Mohammed M, Amjed Adnan A. In-silico design, molecular docking, molecular dynamic simulations, molecular mechanics with generalised born and surface area solvation study, and pharmacokinetic prediction of novel diclofenac as anti-inflammatory compounds. Turkish Comput Theor Chem 2024;8(3):108-121.
5. Helmanto H, Siregar M, Rahmawati SU, *et al*. Exploration of plant diversity at the forest patches in North Sulawesi and their conservation strategy. IOP Conf Ser Earth Environ Sci 2021;948(1):012048.
6. Thomas DC, Ardi WH, Chong YH, *et al*. Conservation status assessments of species-rich tropical taxa in the face of data availability limitations: Insights from Sulawesi Begonia. Sci Rep 2024;14(1):14007.
7. Ardi WH, Zubair MS, Rusdi, Thomas DC. *Begonia medicinalis* (Begoniaceae), a new species from Sulawesi, Indonesia. Phytotaxa. 2019;423(1):41-45.
8. Prihardina B, Fatmawati S. Cytotoxicity of *Begonia medicinalis* aqueous extract in three cancer cell lines. IOP Conf Ser Earth Environ Sci 2021;913(1):012084.
9. Velincia TL, Hayati F, Zubair MS. *Begonia medicinalis*: A review of phytochemistry and pharmacology. J Ilm Farm 2024;20(1):31-42.
10. Zubair MS, Khairunisa SQ, Sulastri E, *et al*. Antioxidant and antiviral potency of *Begonia medicinalis* fractions. J Basic Clin Physiol Pharmacol 2021;32(4):845-851.
11. Ritna A, Anam S, Khumaidi A. Identification of flavonoid compounds in the ethyl acetate fraction of the rock mistletoe (Begonia sp.) from North Morowali Regency. J Farm Galen 2016;2(2):83-89.
12. Hommel U, Hurth K, Rondeau JM, *et al*. Discovery of a selective and biologically active low-molecular weight antagonist of human interleukin-1β. Nat Commun 2023;14:5497.
13. Manakbayeva A, Bogoyavlenskiy A, Kerimov T, *et al*. Gallic, aconitic, and crocetin acids as potential TNF modulators: An integrated study combining molecular docking, dynamics simulations, ADMET profiling, and gene expression analysis. Molecules 2025;30(15):3175.
14. Dallakyan S, Olson AJ. Small-molecule library screening by docking with PyRx. Methods Mol Biol 2015;1263:243-250.
15. Gruin S, Creţu O, Mioc A, *et al*. Evaluation of *Cedrus atlantica* essential oil: Chemical composition, anticancer activity and molecular docking studies. Molecules 2025;31(1):46.
16. Negru PA, Radu AF, Radu A, *et al*. Computational evaluation and multi-criteria optimization of natural compound analogs targeting SARS-CoV-2 proteases. Curr Issues Mol Biol 2025;47(7):577.
17. Goel RK, Singh D, Lagunin A, *et al*. PASS-assisted exploration of new therapeutic potential of natural products. Med Chem Res 2011;20(9):1509-1514.
18. Abdul-Hammed M, Adedotun IO, Olajide M, *et al*. Virtual screening, ADMET profiling, PASS prediction, and bioactivity studies of potential inhibitory roles of alkaloids, phytosterols, and flavonoids against COVID-19 main protease (Mpro). Nat Prod Res 2022;36(12):3110-3116.
19. Lipinski CA. Lead- and drug-like compounds: The rule-of-five revolution. Drug Discov Today Technol 2004;1(4):337-341.
20. Daina A, Michielin O, Zoete V. SwissADME: A free web tool to evaluate pharmacokinetics, drug-likeness and medicinal chemistry friendliness of small molecules. Sci Rep 2017;7(1):42717.
21. Banerjee P, Kemmler E, Dunkel M, *et al*. ProTox 3.0: A webserver for the prediction of toxicity of chemicals. Nucleic Acids Res 2024;52(W1):W513-W520.
22. Verdonk ML, Cole JC, Hartshorn MJ, *et al*. Improved protein–ligand docking using GOLD. Proteins 2003;52(4):609-623.
23. Prastika RA, Putra APE, Fadhana MA, *et al*. In silico identification of organosulfur compounds from *Allium ascalonicum* L. as potential inhibitors of influenza A (H5N1): Integrated DFT, docking, and molecular dynamics analysis. Front Virol 2026;6:1857484.
24. Khumaidi A, Widodo A, Nugrahani AW, *et al*. Lymphocyte cell proliferation profile of Benalu Batu (*Begonia medicinalis*) from the North Morowali Regency, Central Sulawesi Province. J Ilmu Kefarmasian Indones 2020;18(1):61-67.
25. Vadalà M, Laurino C, Palmieri L, *et al*. Shark derivatives (Alkylglycerols, Squalene, Cartilage) as putative nutraceuticals in oncology. Eur J Oncol 2017;22(1):5-20.
26. Micera M, Botto A, Geddo F, *et al*. Squalene: More than a step toward sterols. Antioxidants 2020;9(8):688.

27. Gumus E, Erdogan O, Demirkan B, *et al*. Squalene suppresses Jam-A, Claudin 5, and Occludin by accelerating cell death and reducing neuronal interaction in the neuroblastoma cell line SH-SY5Y. J Res Pharm 2022;26(6):1676-1684.
28. Ciarcià G, Bianchi S, Tomasello B, *et al*. Vitamin E and Non-communicable diseases: A review. Biomedicines 2022;10(10):2473.
29. Bakrim S, Benkhaira N, Bourais I, *et al*. Health benefits and pharmacological properties of stigmasterol. Antioxidants 2022;11(10):1912.
30. Zubair MS, Mutiani RS, Evi S, *et al*. Self-nanoemulsifying drug delivery system (SNEDDS) of ethyl acetate fraction of *Begonia medicinalis* herb and ethanol fraction of *Moringa oleifera* L. leaves. J Nanotechnol 2026;2026:3731383.
31. Maulydia NB, Khairan K, Tallei TE, *et al*. Exploring the medicinal potential of *Blumea balsamifera*: Insights from molecular docking and molecular dynamics simulations analyses. Malacca Pharm 2024;2(1):33-40.
32. Kalita A, Das M, Das B, *et al*. Molecular docking prediction and in vitro studies elucidate anti-inflammatory effect of Garcinia extract against inducible nitric oxide synthase and cyclooxygenase-2 targets. Beni-Suef Univ J Basic Appl Sci 2022;11(1):32.
33. Xia C, Misra I, Iyanagi T, Kim JJ. Regulation of interdomain interactions by calmodulin in inducible nitric-oxide synthase. J Biol Chem 2009;284(44):30708-30717.
34. Moawadh MS. Molecular docking analysis of natural compounds as TNF-α inhibitors for Crohn's disease management. Bioinformation 2023;19(6):716-720.
35. Ibrahim RM, Abdel-Baki PM, Elmasry GF, *et al*. Combinative effects of akarkara root-derived metabolites on anti-inflammatory and anti-alzheimer key enzymes: Integrating bioassay-guided fractionation, GC-MS analysis, and in silico studies. BMC Complement Med Ther 2023;23(1):413.
36. Rahman MO, Ahmed SS, Alqahtani AS, *et al*. Identification of stigmasterol derived AChE inhibitors for Alzheimer's disease using high throughput virtual screening and molecular dynamics simulations. Sci Rep 2025;15(1):36676.